Atmosphere **2012**, *3*, 103-123; doi:10.3390/atmos3010103

OPEN ACCESS

atmosphere

ISSN 2073-4433

www.mdpi.com/journal/atmosphere

Article

An Evaluation of Modeled Plume Injection Height with Satellite-Derived Observed Plume Height

Sean M. Raffuse [1,*], Kenneth J. Craig [1], Narasimhan K. Larkin [2], Tara T. Strand [2,†], Dana Coe Sullivan [1], Neil J. M. Wheeler [1] and Robert Solomon [2]

[1] Sonoma Technology, Inc., 1455 North McDowell Blvd., Suite D, Petaluma, CA 94954, USA; E-Mails: kcraig@sonomatech.com (K.J.C.); dana@sonomatech.com (D.C.S.); neil@sonomatech.com (N.J.M.W.)

[2] USDA Forest Service AirFire Team, 400 North 34th Street, Suite 201, Seattle, WA 98103, USA; E-Mails: larkin@fs.fed.us (N.K.L.); tarastrand@fs.fed.us (T.T.S.); robertsolomon@fs.fed.us (R.S.)

† Present Address: Scion Research, 49 Sala Street, Rotorua 3046, New Zealand.

* Author to whom correspondence should be addressed; E-Mail: sraffuse@sonomatech.com; Tel.: +1-707-665-9900; Fax: +1-707-665-9800.

Received: 14 October 2011; in revised form: 17 December 2011 / Accepted: 6 January 2012 / Published: 18 January 2012

Abstract: Plume injection height influences plume transport characteristics, such as range and potential for dilution. We evaluated plume injection height from a predictive wildland fire smoke transport model over the contiguous United States (U.S.) from 2006 to 2008 using satellite-derived information, including plume top heights from the Multi-angle Imaging SpectroRadiometer (MISR) Plume Height Climatology Project and aerosol vertical profiles from the Cloud-Aerosol Lidar with Orthogonal Polarization (CALIOP). While significant geographic variability was found in the comparison between modeled plumes and satellite-detected plumes, modeled plume heights were lower overall. In the eastern U.S., satellite-detected and modeled plume heights were similar (median height 671 and 660 m respectively). Both satellite-derived and modeled plume injection heights were higher in the western U.S. (2345 and 1172 m, respectively). Comparisons of modeled plume injection height to satellite-derived plume height at the fire location (R^2 = 0.1) were generally worse than comparisons done downwind of the fire (R^2 = 0.22). This suggests that the exact injection height is not as important as placement of the plume in the correct transport layer for transport modeling.

Keywords: plume injection height; biomass burning; CALIPSO; MISR; aerosol

1. Introduction

During the past decade, there has been an increase in both the number and intensity of wildfires in the western U.S. and the wildfire season is expected to lengthen as temperatures warm [1]. In addition, U.S. air quality regulations have been tightening. Due to these regulations, attention has been focused on modeling and forecasting smoke impacts from wildfires and efforts are underway to develop and improve smoke modeling and forecasting systems [2–6] that can accurately predict smoke impacts on visibility and concentrations of pollutants of concern to human health.

For this paper, we define plume injection height and plume top as the vertical zone in which a buoyant plume begins to transport horizontally away from its source, and the top of that zone respectively. Plume injection height is important for modeling wildfire smoke plume transport, footprints, and surface concentrations. The injection height of the plume determines the type of winds and turbulence the plume will experience. For example, extremely buoyant wildfire smoke columns produce plumes that break through the atmospheric boundary layer and are transported hundreds to thousands of kilometers downwind in the free-stream transport winds [7,8]. In contrast, smoke plumes remaining within the boundary layer often become well-mixed in regions near a fire [9]. A wildfire smoke column may have several plume injection heights and this vertical distribution of plume mass is a key input for dispersion and air quality models. Model results, such as surface concentrations, are sensitive to the amount of plume mass injected at various heights because the associated winds and turbulence directly influence the plume footprint and dilution. Accurately characterizing smoke plumes and their vertical structures is necessary to produce useful local-, regional-, and national-scale smoke predictions.

Buoyant plume injection height is a function of both the heat release rate from the source and the prevailing meteorology [10]. The rate of heat release is directly related to the rate of biomass consumption. Unfortunately, estimates of biomass consumption for a given fire are highly uncertain [2,5,11,12]. Moreover, the amount and rate of heat release from fires varies by combustion phase making hourly heat release difficult to estimate. Even if all of the physical parameters for a specific fire are well known, modeling plume injection height is difficult due to the difference between the spatial resolution of the model and the scale of the variation of the burn activity. Finally, wildfires often occur over a large area, and within that area differences in terrain, vegetation, and fuel moisture lead to different consumption characteristics. This heterogeneity often leads to the total heat released splitting into several plume cores [13].

Previous studies have identified a need to improve the spatial and temporal characterization of heat release from fires [4,14]. Efforts are underway to quantify the uncertainties associated with smoke modeling and develop algorithms that are more representative of real-world smoke transport [9,10,15–17]. However, due to the difficulty of acquiring information about plume height from real fires, there has been a lack of data to compare observed plume heights with model estimates.

One way to characterize smoke plume behavior is through the use of information derived from satellite data. In recent years, satellite data products were used to evaluate the vertical structure and smoke plume characteristics of wildland fires. Several research efforts have characterized smoke plumes from observations with the goal of improving model performance [18–21], but most comparisons to model outputs have been limited to case studies, with one recent exception [22]. This paper describes a study that compared plume height data derived from the MISR onboard Terra and the CALIOP onboard the Cloud-Aerosol Lidar and Infrared Pathfinder Satellite Observation (CALIPSO) satellite against modeled plume height estimates for a large number of fires in the U.S. from 2006 through 2008. The use of both MISR and CALIOP provides complementary information [23]. To our knowledge, it is the first study that compares CALIPSO data to multiple modeled smoke plumes beyond individual case studies.

2. Methods

Plume top height data collected by MISR and CALIOP were compared to the modeled vertical mass distribution for 227 fires and their plumes that occurred from 2006 through 2008 in the contiguous U.S.

The overall technical approach for this work involved four general steps: (1) data acquisition and processing; (2) identification of fires and corresponding CALIOP and MISR satellite observations from 2006 through 2008; (3) production of modeled smoke predictions for comparison to the satellite observations; and (4) comparison and assessment of the modeled plume height predictions to the satellite derived observations.

2.1. Data Acquisition and Processing

MISR and CALIOP measure plume heights in distinct and complementary ways. MISR relies on stereoscopic analysis of plumes based on a minimum of two angular views to extract plume heights [18]. The CALIOP instrument uses active lidar to measure aerosol vertical profiles [24].

In addition to the satellite data, several other sources of data and software applications were used to acquire and prepare the data used for this study:

- The Hazard Mapping System (HMS) Smoke Product [25] was used to identify when and where smoke plumes were present from 2006 through 2008 [26].
- Daily fire locations from the Satellite Mapping Automated Reanalysis Tool for Fire Incident Reconciliation (SMARTFIRE) fire information system [27] were used to identify latitudinal and longitudinal locations of fires and burn area estimates for fires present from 2006 through 2008 [28].
- The Satellite Nadir Track Sensor Observation Service provided by the Vis Analysis Systems Technologies team at the University of Alabama in Huntsville [29] was used to determine CALIPSO orbit paths and identify days when these paths intersected a smoke plume in the HMS data set.
- CALIOP Lidar Level-2 5 km aerosol data acquired from the Atmospheric Science Data Center (ASDC) [30] were used to compare observed smoke plume heights to modeled plume heights [31].

- CALIOP Lidar Level-1B 532 nm wavelength attenuated backscatter data were acquired from the ASDC and used for data visualization and qualitative assessment of smoke plume characteristics and $PM_{2.5}$ concentrations.
- Smoke plume summary data acquired from the MISR Plume Height Climatology Project [32] were used to compare observed smoke plume heights to modeled plume heights [33]. Specifically, we used the median wind corrected plume heights.
- The BlueSky framework smoke modeling system was used to develop smoke plume height and fire emission and heat estimates for comparison to the CALIOP and MISR satellite observations [2].
- The Community Multiscale Air Quality (CMAQ) model was used to transport and diffuse injected smoke plumes to compare with CALIOP aerosol data [34].

2.2. Identification of Fires and Corresponding MISR and CALIOP Satellite Observations

The HMS database was used to identify satellite detectable smoke plumes from fires from 2006 through 2008. The HMS data set includes daily electronic (GIS-based) maps of smoke plume extents as determined and digitized by trained satellite analysts. HMS analysts examine operational satellite imagery, particularly from MODIS and GOES, and qualitatively delineate visible areas of smoke. The SMARTFIRE information system was used to query fire information including fire location and area burned estimates for days and times corresponding to the HMS smoke plume data. SMARTFIRE integrates and reconciles human-recorded wildfire incident data from Incident Status Summary (ICS-209) reports with satellite-detected fire data from by HMS. The HMS fire data set is a combination of automated fire detection and human quality control. It includes automated fire detections from two geostationary satellites (GOES-East and GOES-West) and five polar orbiting satellites (Moderate Resolution Imaging Spectroradiometer [MODIS] Terra and Aqua and the Advanced High-Resolution Radiometer [AVHRR] on three NOAA spacecraft).

Next, the SMARTFIRE datas were used to query the MISR plume height satellite observation database for days and times that correspond to the SMARTFIRE data set. The MISR Plume Height Climatology Project data archive contains information about North American smoke plume characteristics for 2002 and from 2004 through 2007. The native data set consists of 61 smoke plume parameters corresponding to a single geographic coordinate location. The following MISR parameters were acquired for this study: plume location (latitude and longitude) and date, median and maximum plume height, median and maximum wind corrected plume height, and median and maximum wind corrected plume height using a planar correction. The MISR plume height data were matched to fires from the SMARTFIRE database by date and location. Matched MISR-SMARTFIRE plumes were determined by selecting the nearest same-day fire location in the SMARTFIRE database (within 10 km) for fires greater than 40.5 hectares (100 acres). A total of 163 records from the MISR plume height database were matched to SMARTFIRE fire locations for comparison.

CALIOP satellite data were acquired based on days and times when the CALIPSO satellite orbit path intersected an HMS smoke plume. Daily CALIPSO orbit path data were overlaid with daily HMS smoke plume data for 2006 through 2008 and the geographic intersection points were recorded as candidate times and locations when the satellite was likely to detect a smoke plume. For days with

CALIPSO-smoke plume intersections, map images were created and inspected. Because this study is concerned with plume injection height rather than plume transport, we preferentially selected days when the CALIPSO orbit path was close to the origin of a smoke plume, as determined by the SMARTFIRE fire locations. The maximum allowed distance between the CALIPSO orbit path and the fire origin was 50 km. Figure 1 shows an example of the process for identifying days and times when the CALIPSO orbit paths intersected HMS smoke plumes.

Figure 1. Example of the method for identifying days and times when the CALIPSO orbit path intersected an HMS smoke plume. The HMS smoke plume data are indicated by blue shading, the CALIPSO orbit paths are shown as green lines, and red circles are the SMARTFIRE fire locations. Red lines indicate times when the CALIPSO orbit path intersected the HMS smoke plume.

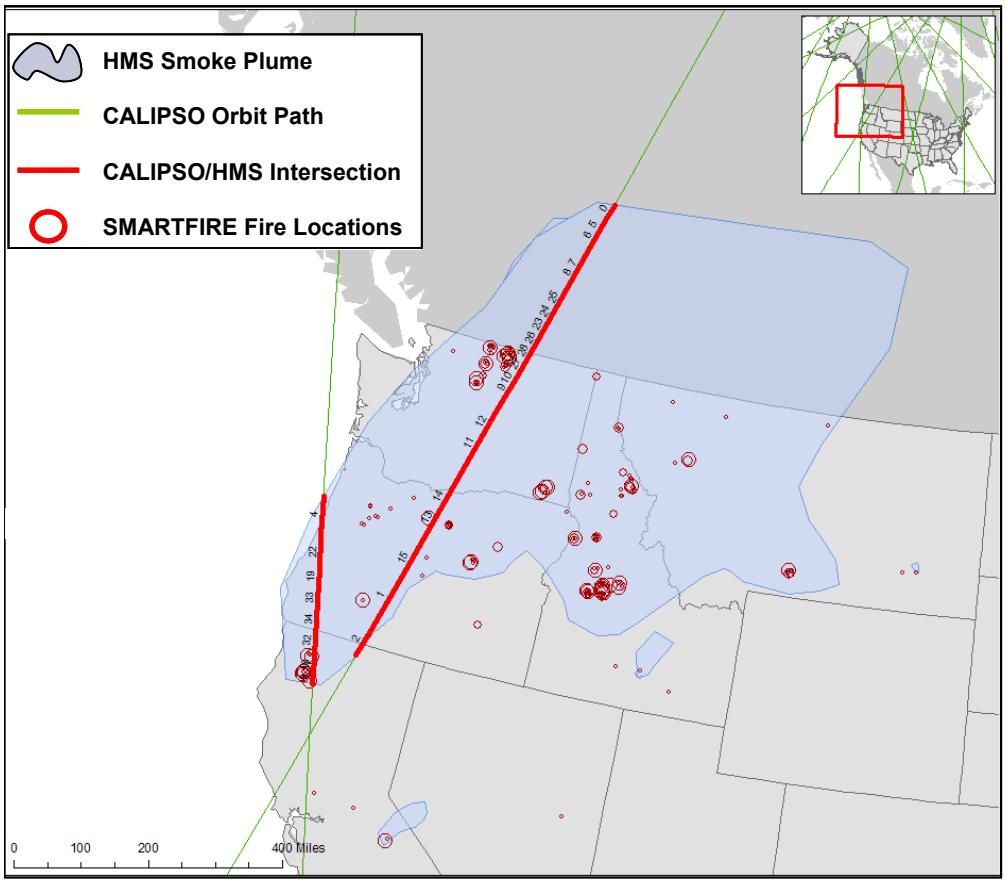

A total of 157 CALIPSO orbit paths (out of 25,000 orbits during the time period of interest) intersected HMS smoke plumes for 2006 through 2008. For the 157 CALIPSO orbit paths, the following data were acquired from the CALIOP instrument: level-1 532 nm attenuated backscatter data, and level-2 aerosol data averaged over 5 km (along the ground).

2.3. Development of Modeled Smoke Predictions

Heat and emissions from wildland fires can be estimated as shown below in Equation (1) [35]:

$$M(x) = A \times AFL \times \beta \times Ef(x) \quad (1)$$

Where: $M(x)$ is the heat or mass emitted of species x; A is the area burned; AFL is the available fuel load including live and dead vegetation and soils in mass per unit area; β is the burning efficiency or the fraction of fuel consumed, and $Ef(x)$ is the emission factor for heat release (energy emitted per mass of fuel consumed) or for chemical species x (mass of chemical species x emitted per mass of fuel consumed).

The BlueSky modeling framework [2] was used to construct the modeling pathway. The BlueSky framework links many different model applications together to produce emissions and pollutant transport estimates from wild and prescribed fires. Figure 2 illustrates the process pathway and model applications that were used to estimate emissions and generate the aerosol mass distribution predictions to compare to the satellite observations.

Figure 2. Model pathway used to develop estimates of plume height and smoke predictions for comparison to MISR and CALIOP observations. FCCS, Consume3.0, and FEPS are used as implemented in the BlueSky Framework, version 3.0.0 [36]. [1] Sullivan, *et al.* (http://www.getbluesky.org/smartfire) [37]; [2] Fuel Characterization Classification System (FCCS) (http://www.fs.fed.us/pnw/fera/fccs/) [38]; [3] Consume 3.0 [39]; [4] Fire Emission Production Simulator (FEPS) (http://www.fs.fed.us/pnw/fera/feps/index.shtml) [40]; [5] Sparse Matrix Operating Kernel Emissions (SMOKE), version 2.3 [41]; [6] Community Multiscale Air Quality (CMAQ) model, version 4.5.1 [42].

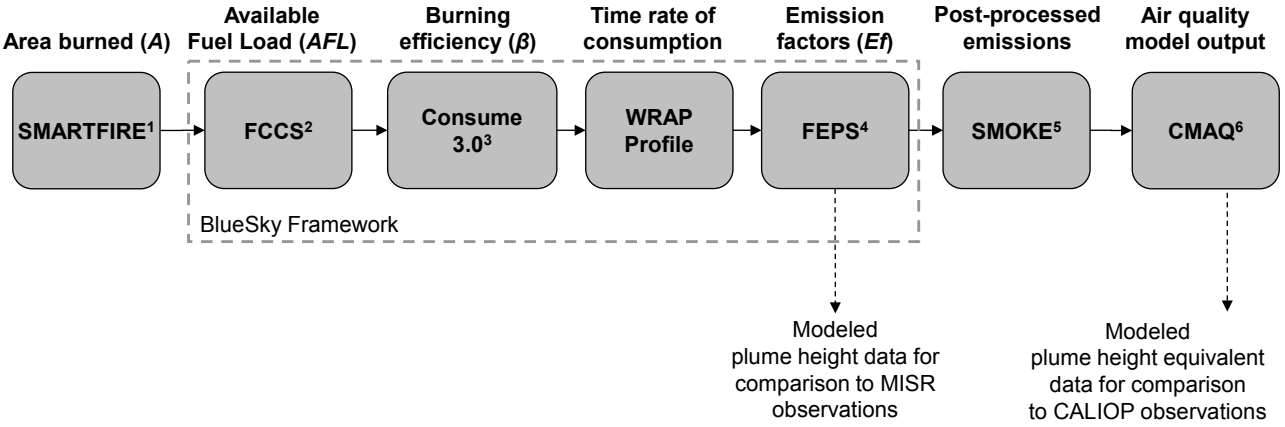

This study employed the most recent smoke modeling systems available in the BlueSky framework to calculate each term in the emission equation. Available fuel load was calculated using the Fuel Characterization and Classification System (FCCS) [43,44], which provides a map of over 100 fuelbed models at 1-km resolution. Biomass consumed was calculated using Consume 3.0 [39], which combines fuelbed information and weather data to produce estimates of fuel consumption by burn phase (*i.e.*, flaming, smoldering, and residual) and fuel bed strata (e.g., forest canopy, soil, ladder fuels). Daily bulk consumption was then allocated hourly using a time profile developed by the Western Regional Air Partnership (WRAP) [45]. Emissions factors, including heat, were modeled using the Fire Emission Production Simulator (FEPS) [40], which modulates emission factors based on combustion efficiencies. Results of this modeling included hourly emissions and heat release rates for each fire studied. Plume injection heights were calculated using Briggs plume rise methods for buoyancy-dominated plumes [46] as implemented in FEPS. Briggs plume rise is a function of buoyancy, ambient wind speed, and static stability. FEPS computes the buoyancy parameter as 2.58×10^{-6} times the heat release rate. Heat

release is calculated as shown in Equation 1 and, therefore, depends on all previous modeling steps. The wind speed was defined by the BlueSky default value of 6 mph. Pasquill stability class [47] is set to unstable (stability class A) during daytime hours (defined as 0600 to 1800 local), and ranges from slightly unstable to slightly stable (stability class C through E) during nighttime hours depending on wind speed. The Briggs stability parameter is based on the vertical temperature gradient that FEPS defines based on Pasquill stability class. The FEPS injection height calculator produces hourly estimates of the plume top for each fire.

The modeled plume top data were used to compare to median wind corrected heights from the MISR plume height climatology project. The MISR heights are based on fitting a plane to the wind corrected heights derived at each pixel within an identified plume, removing all points more than 1.5 standard deviations from the plane, and taking the median of the remaining points [33].

Because the CALIOP footprint is so narrow, it rarely passes directly over a fire. CALIOP plume detections typically occur downwind of the source fire. Therefore, it was not possible to distinguish plume injection height from plume transport in the CALIOP data set. To compare the CALIOP plume data to modeled plume data, the CMAQ model (CMAQ version 4.5.1 was used for this study) [42] was used to generate downwind plume heights and $PM_{2.5}$ concentrations for fires corresponding to the CALIOP data set.

The Sparse Matrix Operating Kernel Emissions (SMOKE) system, version 2.3, [41] was used to post-process emissions estimates from FEPS to create CMAQ-ready emissions data files that contain spatially and temporally resolved emissions estimates [48–51]. The output of the SMOKE system was a field of vertically distributed fire emissions, which were merged with day-specific biogenic and anthropogenic emissions, generated using SMOKE to produce the final merged three-dimensional emissions input files for the CMAQ model. Emissions estimates of heat release and several primary pollutants (e.g., $PM_{2.5}$, CO, sulfur dioxide [SO_2], NO_x) were produced for input to the CMAQ model.

The CMAQ model was used to produce three-dimensional fields of $PM_{2.5}$ concentrations from fires during 2006 through 2008 on the national 36-km Regional Planning Organization grid, covering the contiguous U.S. The model simulations are driven by meteorological data from Version 3.7 of the Fifth-Generation Pennsylvania State University/National Center for Atmospheric Research mesoscale model (MM5). The MM5 modeling was performed on a 29-layer vertical grid, with vertical resolution of 50 to 75 m in the lower troposphere gradually stretching to coarser resolution at the upper layers of the grid. The CMAQ modeling was performed on a 17-layer vertical grid, which aligns with the MM5 vertical grid.

To compare the CMAQ model output with the CALIOP observations, vertical profiles of $PM_{2.5}$ concentrations from wildfires were extracted from the model output. These concentrations were bi-linearly interpolated from the four nearest grid cell centers to the satellite orbit path locations. The CALIOP orbit paths were matched to the CMAQ modeled data by day and time. Data were eliminated for times when a one-to-one match between the CALIOP and CMAQ data could not be made. A total of $N = 64$ CALIOP-CMAQ data pairs were included in the analysis and the modeled $PM_{2.5}$ concentration data were compared to the CALIOP aerosol data for the data pairs. Figure 3 shows an example of the comparison of the CALIOP aerosol data and the CMAQ modeled $PM_{2.5}$ concentrations.

These comparisons were made to qualitatively examine the spatial distribution, extent, and concentrations of $PM_{2.5}$ plumes produced by the CMAQ model.

Figure 3. Example of matched profiles for CALIOP 532 nm total attenuated backscatter data (top), CALIOP aerosol layers (middle), and $PM_{2.5}$ concentrations from the BlueSky—CMAQ modeling system (bottom) for 28 August 2006.

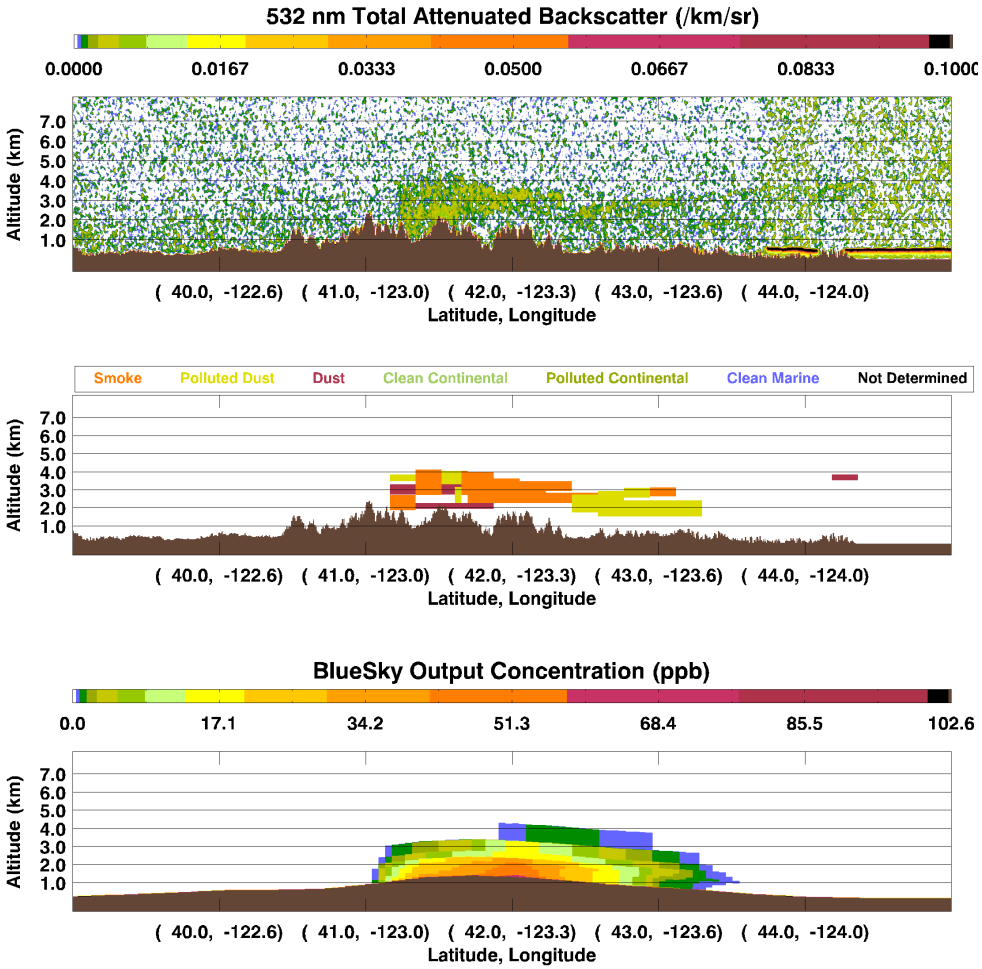

Plume height information from the CALIOP data was compared with plume height information from the CMAQ model. For CALIOP, plume top height was calculated as the average of the maximum heights in the aerosol feature mask product. The CMAQ model output does not explicitly contain plume top data. To allow the comparison of the CMAQ modeled data and the CALIOP plume height data, a CMAQ plume top equivalent value was derived. The CMAQ model generates predictions of three-dimensional pollutant concentrations as they undergo transport, chemical transformation, and dispersion. Concentrations of $PM_{2.5}$ from smoke are typically highest slightly above the location from which they are emitted. As a smoke plume rises vertically, atmospheric dispersion and mixing cause pollutant concentrations to decrease. The CMAQ plume height equivalent was derived by identifying the vertical height at which the modeled $PM_{2.5}$ concentration was 10% of the maximum $PM_{2.5}$ concentration within the vertical column. Use of a threshold is necessary because vertical diffusion in a coarse vertical grid structure mixes small amounts of $PM_{2.5}$ to altitudes well above the bulk of the modeled plume. The selection of this threshold is arbitrary, and changing its value would affect biases in

predicted plume top height; however, other threshold values investigated had minimal effect on the overall correlation. Figure 4 is a conceptual illustration of the methodology used to derive the CMAQ plume top equivalent.

Figure 4. Conceptual illustration of the methodology used to derive the CMAQ plume top equivalent.

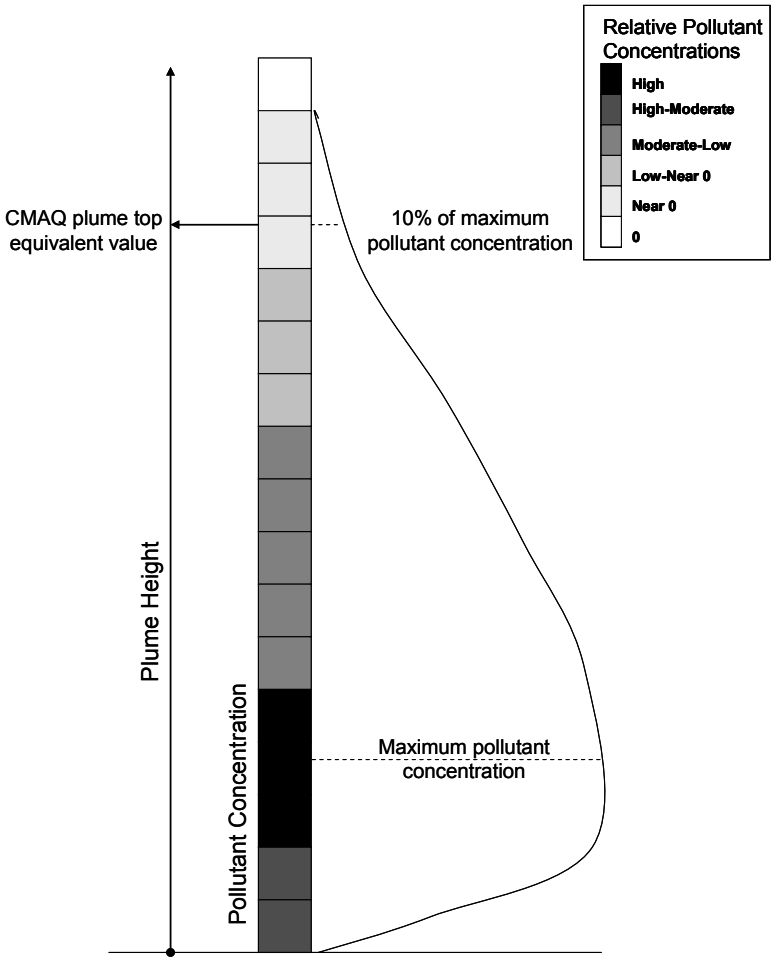

2.4. Statistics and Analysis Used in Comparing Plume Heights

Statistical analyses were performed to compare the extent to which observed plume heights from the MISR and CALIOP data agreed with the FEPS and CMAQ model results, respectively. Basic descriptive statistics (e.g., mean, median, standard deviation) were calculated for each data set. For each comparison, a Kolmogorov-Smirnof test was performed to determine the statistical significance between the satellite-derived and modeled plume height data. The data were also analyzed by region to determine if there was a regional influence on the statistical results. Plume height estimates were further investigated by examining parameters that drive the plume injection height calculations, such as area burned and fuel loading.

3. Results

3.1. Comparison of MISR Observed Plume Heights to FEPS Plume Heights

Results of the comparisons between the MISR observed plume heights (median wind corrected) and the FEPS modeled plume heights show that the satellite-derived plume-top height has statistically significantly ($p < 0.01$) higher median value than the modeled plume-top height (Table 1). In addition, the overall range of the modeled plume heights was larger than the range of observed plume heights. Examining the paired data for all the individual plumes shows that there is only a weak correlation between the data sets ($r^2 = 0.1$). Figure 5 shows the results of the regression analysis for the observed plume heights (x-axis) *versus* the modeled plume heights (y-axis). Other studies have found better correlation using MISR maximum wind corrected heights instead of median wind corrected heights [52]; however, our results using the maximum wind corrected height were slightly worse ($r^2 = 0.09$).

Table 1. Comparison of the overall distributions of observed median wind corrected plume top heights from the MISR instrument and modeled plume top heights from FEPS. Plume height units are meters (m) above ground level.

Parameter (units)	MISR Plume Top Height Observations	FEPS Modeled Plume Top Height
Number of samples	163	163
Minimum (m)	284	109
Maximum (m)	5,088	18,699
Median (m)	1,436	806
Mean (m)	1,699	1,557
Standard Deviation (m)	1,124	2,116

Figure 5. Regression analysis results for modeled plume heights (y-axis) *versus* the MISR observed plume heights (x-axis). Data points are color coded by region as shown on Figure 6. Also shown on the plot are the linear regression (solid line) and 1:2, 1:1, and 2:1 lines (dotted black lines). Note that a single value is off scale and not shown (MISR height = 2312 m; Modeled height = 18,699 m).

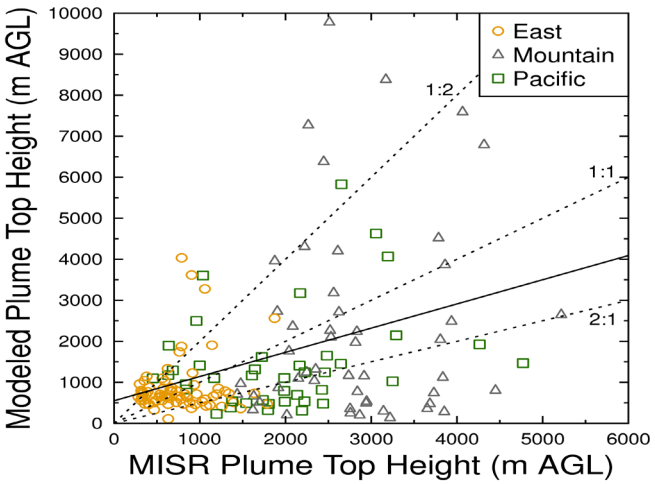

While there was little correlation between MISR observed and FEPS modeled plume heights when all data values were considered, the spatial distribution of modeled and observed plume heights across the U.S. agree qualitatively. The data points in Figure 5 are broken out by three regions, delineated in Figure 6. There are several differences between the fire regimes in the southeastern and western U.S., including the type, density, and moisture of the vegetation. In addition, most of the area burned in the Southeast is the result of prescribed fires, while there is a much higher occurrence of wildfires in the western U.S. [53]. Wildland fires in the southeastern U.S. generally produce lower plume heights compared to those in the western U.S. The difference between observed and modeled plume heights is larger in the mountain and Pacific Northwest regions, where the median observed plume heights are statistically significantly greater than the modeled plume heights but some modeled plume heights are several times higher than those observed by MISR. In the Southeast, there is no statistically significant difference between observed and modeled plume heights. Distribution statistics by region are given in Table 2.

In our modeling, plume injection height is controlled by heat release, which is in turn driven by a combination of area burned, fuel loading, and combustion efficiency. The assumed diurnal time profile also affects the heat released, but this effect is constant among all fires. Because area burned and fuel loadings are highly variable, we examined the FEPS modeled plume injection height compared to the MISR observations as a function of modeled area burned and fuel loading.

Figure 6. Map of the fire locations and corresponding plume height data from the modeled (red bars) and satellite derived (blue bars) data. Regions are color coded to match data points shown in Figure 5.

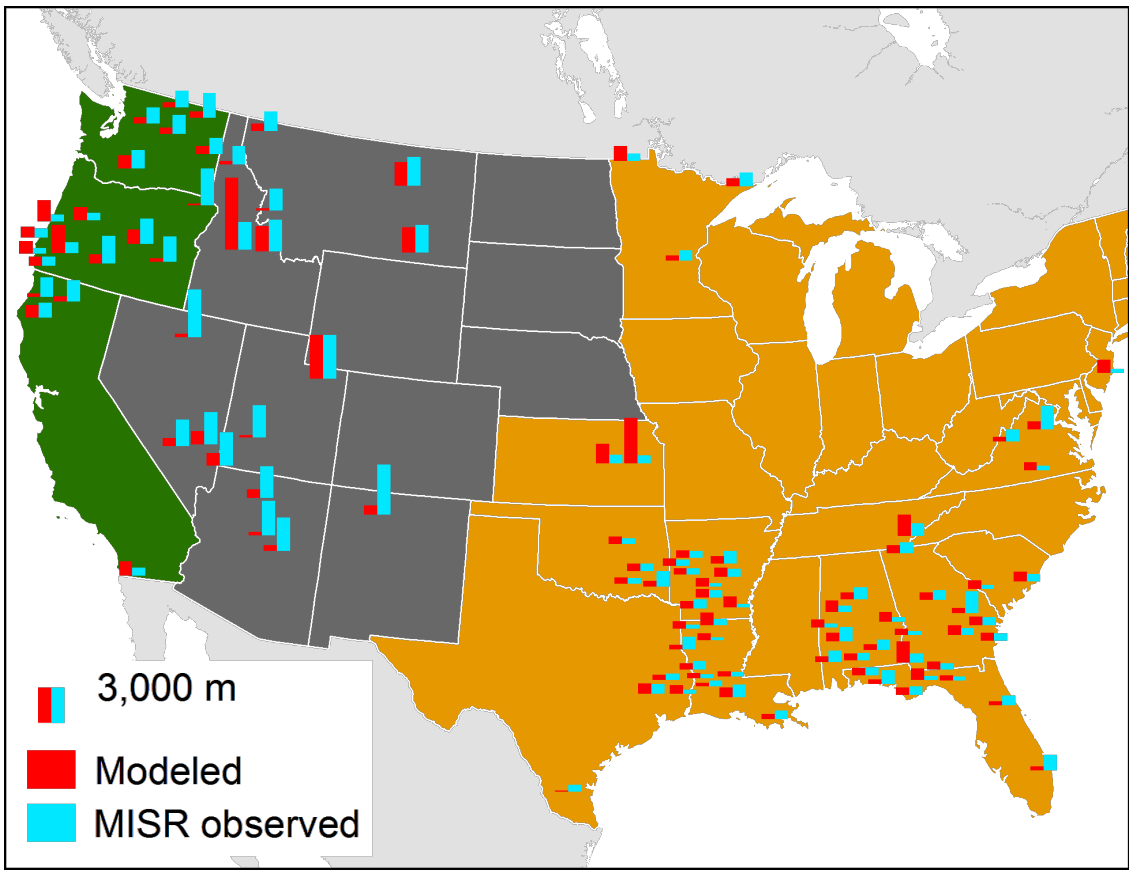

Table 2. Comparison of the overall distributions of observed median wind corrected plume top heights from the MISR instrument and modeled plume top heights from FEPS by region. Plume height units are meters (m) above ground level. Region definitions are shown in Figure 6.

Parameter (units)	West		Central		East	
	MISR	FEPS	MISR	FEPS	MISR	FEPS
Number of samples	42	42	50	50	71	71
Minimum (m)	452	231	1,436	138	284	109
Maximum (m)	4,770	18,699	5,216	9,781	1,872	4,033
Median (m)	1,984	1,172	2,745	1,209	798	660
Mean (m)	1,960	1,861	2,824	2,276	768	871
Standard Deviation (m)	948	2,923	856	2,378	371	704

Estimates of area burned have a significant impact on the FEPS modeled plume injection height (Figure 7). Modeled plume heights for fires with an area burned of fewer than 800 hectares (1976 acres) are significantly lower than the MISR observed plume heights for the same fires. Likewise, modeled fires with an area burned greater than 2000 hectares (4940 acres) produced plume rises much greater than MISR observed data.

Figure 7. Notched box-whisker plot of modeled (red) and MISR observed (blue) plume heights as a function of modeled area burned. The notch is centered on the median concentration, widening to the size of the box to illustrate a 95% confidence interval in the median concentration value. The edges of the box illustrate 25th and 75th percentile concentrations. The whiskers indicate the lowest and highest values that are within 1.5 times the interquartile range (IQR). Outliers (denoted by plus signs) fall between 1.5 and 3 times the IQR.

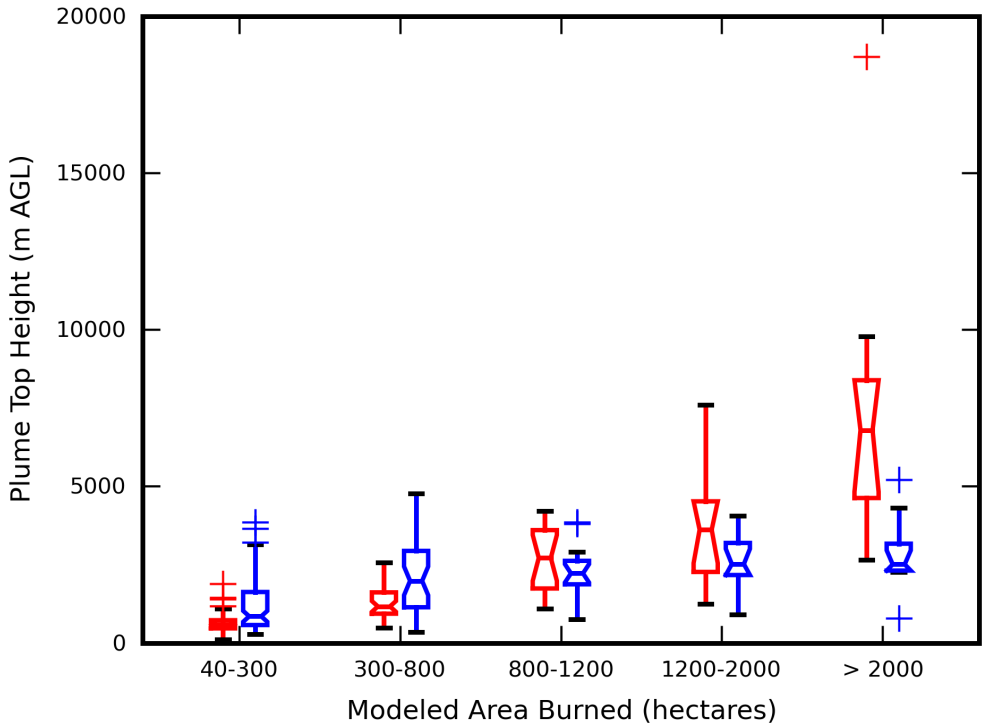

Fuel loading is the total biomass available to burn per unit area of land. Fuel loading values vary greatly across the U.S. and sometimes within individual fires. The plume height model was examined to determine how it performs under different fuel loading scenarios. Figure 8 shows a notched box-whisker plot of the modeled (red) and observed (blue) plume height as a function of fuel loading. For fires with fuel loading values of about 2.25 kg of fuel/square meter (10 tons/acre) or less, the median observed plume height was statistically significantly higher than the median modeled plume height. For fires with fuel loading values greater than 2.25 kg/square meter, there was no statistically significant difference between the modeled and observed median plume height.

Figure 8. Notched box-whisker plot of the modeled (red) and MISR observed (blue) plume heights as a function of modeled fuel loading.

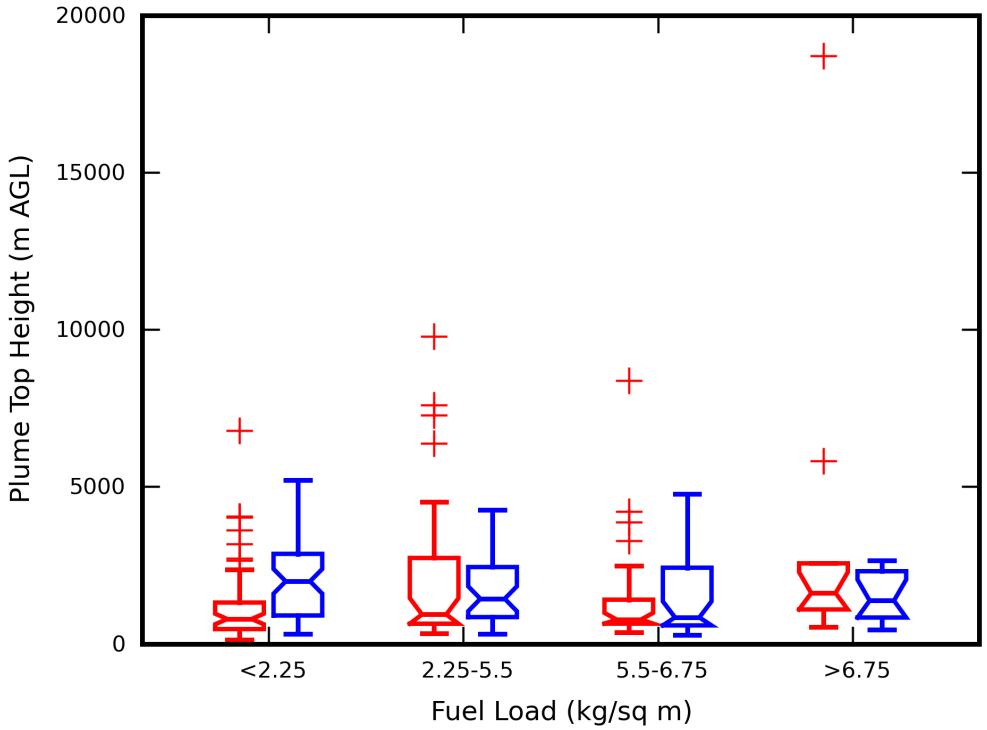

3.2. Comparison of CALIOP Observed Plume Heights to CMAQ Modeled Plume Heights

Table 3 shows the results of the statistical comparison between the CALIOP observed plume height and the CMAQ modeled plume height equivalent. The median CMAQ plume height equivalent was statistically significantly lower than the median CALIOP observed plume height. The range of plume height values was similar; however, the distribution of plume height values was significantly different ($p = 0.005$). A weak but positive correlation was observed between the CALIOP observed plume height and the CMAQ plume height equivalent ($R^2 = 0.22$). Figure 9 shows the results of the regression analysis of the CALIOP observations (x-axis) and the modeled plume height data (y-axis). While there was significant scatter in the results, most of the modeled results (>90%) are within a factor of two difference of the CALIOP observations.

Table 3. Comparison of the overall distributions of observed plume top heights from the CALIOP instrument and modeled plume heights from CMAQ as in Table 1. Plume height units are meters above ground level.

Parameter (units)	CALIOP Plume Height Observations	CMAQ Modeled Plume Height
Number of samples	64	64
Minimum (m)	824	744
Maximum (m)	3,320	3,626
Median (m)	1,940	1,540
Mean (m)	2,033	1,659
Standard Deviation (m)	608	627

Figure 9. Results of the regression analysis of the CALIOP observations (*x*-axis) and the modeled plume height data (*y*-axis). Data points are color coded by region as shown on Figure 10. Also shown on the plot are the linear regression (solid line) and 1:2, 1:1, and 2:1 lines (dotted black lines).

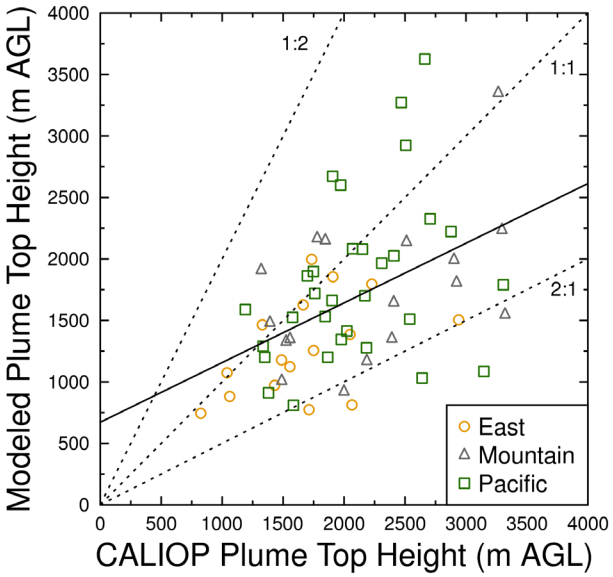

The spatial pattern of plume heights in the CALIOP-CMAQ data set is shown by different symbols in Figure 9 and on a map in Figure 10. There was no significant difference between the CALIOP and CMAQ data by region. Figure 10 shows a map of the fire locations and corresponding plume height data from the CALIOP observations (green bars) and the modeled plume heights (orange bars). Qualitatively, the CMAQ model compares favorably with the CALIOP measurements in some regions, such as central Idaho. Distribution statistics are not provided by region for the CALIOP analysis due to the small sample size.

Figure 10. Map of the fire locations used for the comparison of CALIOP observed plume heights (blue bars) to modeled plume heights (red bars). Regions are color coded to match data points shown in Figure 9.

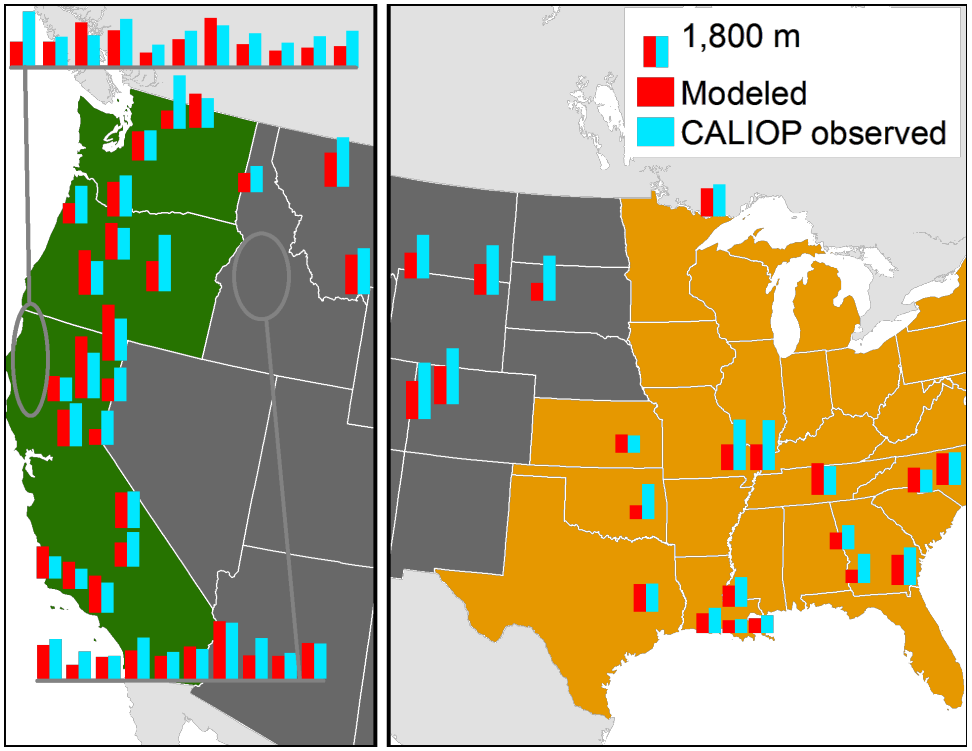

4. Discussion and Conclusions

We compared plume injection height estimates from the default model path within the BlueSky Framework predictive modeling system to a MISR-derived database of plume top heights and CALIOP aerosol vertical profiles. MISR and CALIOP are unique in their ability to vertically resolve atmospheric aerosol signals globally and are thus ideally suited to observing wildland fire plume injection height and evaluating modeled plume injection heights.

On average, our modeled smoke plume tops were lower than the observed plume tops derived from both MISR and CALIOP. The modeled plume tops exhibited much greater variability than the MISR heights and there was a weak correlation between the two data sets. We also input the modeled plume tops into a chemical transport model and compared the resulting vertical profiles with CALIOP aerosol data. These data were weakly correlated and the modeled plume heights were lower than the CALIOP heights.

When examined regionally, the difference between observed and modeled plume tops of wild and prescribed fires that occurred in the southeastern U.S. was not significant; however, the observed and modeled plume heights in the Northwest were significantly different. In addition, under certain circumstances, modeled plume heights of fires in the Northwest were extremely high. These higher plume height differences tended to occur when the size of a fire, or the area burned, was very large.

The regional differences in observed and modeled plume heights do not appear to be solely the result of vegetation and fuel loading. In the Southeast, fires tend to be relatively small, many of which are controlled or prescribed burns. Small and/or controlled burns tend to be less variable than large,

uncontrolled fires. Because the factors that affect plume height tend to be less variable and more bounded, the plume height algorithms produce consistent results for fires in the Southeast.

Fire burn areas in the Northwest tend to be much larger, with lower fuel moisture and more diverse vegetation, or fuel loading. Fires with large burn areas and overall low fuel moistures produce significant heat, which greatly affects plume height in the plume injection height algorithm. Also, as large fires burn heterogeneously in multiple locations, the total heat released is divided into multiple plume cores, resulting in lower heat released per plume and lower plume injection heights [54]. A key factor for large fires that is not considered in the assessed approach is the interaction of the plume with the ambient atmosphere. More sophisticated approaches are being applied in other modeling systems [55] and should be explored. However, the key variables necessary to drive plume injection height models, such as heat flux and the number of independent plume cores within a wild or prescribed fire, remain unavailable for predictive models.

The Briggs approach to plume height calculations depends on heat release, atmospheric stability, and wind speed. The use of default diurnal profiles of atmospheric stabilities and static wind speed in the calculation of plume injection heights is a weakness in the current modeling system. The plume height equivalent data from the model post-transport (CMAQ) showed less variability than the plume height data from the model pre-transport (FEPS) when compared to remotely sensed plume heights. In many cases plume heights were modeled well above the atmospheric boundary layer. While some smoke plumes are injected into the free troposphere in reality [56], most smoke within our modeling domain remains within the boundary layer. val Martin, *et al.* [20] estimated that 4–12% of plumes from fires are injected above the boundary layer in North America, although that includes the more energetic boreal fires of Canada and Alaska.

There is a lack of available data for the parameters that drive heat-release and plume-rise estimates. Existing plume height algorithms and dispersion models attempt to calculate plume injection height based on a series of physical processes to estimate heat emissions estimates, and some include atmospheric processes, but they are hampered by both a lack of available inputs and limited availability of observed data to test process-based algorithms. The Briggs equations underlying the modeled heights used here are commonly used in many different dispersion and air quality modeling systems. To improve this method for wildland fires, the inclusion of dynamic wind speed and atmospheric stability should be explored. In the absence of dynamic meteorology, average, region-specific plume injection heights may be a more representative technique, particularly in the case of large wildfires that burn across large areas of heterogeneous terrain. As new methods and approaches are developed, MISR and CALIPSO can both provide useful comparison data sets.

Acknowledgments

This work was sponsored by a NASA Applied Sciences cooperative agreement (NNS06AB52A). Additional funding was provided by the Joint Fire Science Program (JFSP) as part of the Smoke and Emissions Model Intercomparison Project (SEMIP) (JFSP project id: 08-1-6-10). The authors wish to thank David Diner at the NASA Jet Propulsion Laboratory for providing guidance on the use of MISR plume height data. Finally, the authors wish to acknowledge the intelligence and hard work of Jordan Stone and Katie Wade.

References

1. Westerling, A.L.; Cayan, D.R.; Swetnam, T.W. Warming and earlier spring increase western U.S. forest wildfire activity. *Science* **2006**, *313*, 940–943.
2. Larkin, N.K.; O'Neill, S.M.; Solomon, R.; Raffuse, S.; Strand, T.M.; Sullivan, D.C.; Krull, C.; Rorig, M.; Peterson, J.; Ferguson, S.A. The BlueSky smoke modeling framework. *Int. J. Wildland Fire* **2009**, *18*, 906–920.
3. O'Neill, S.M.; Larkin, N.K.; Hoadley, J.; Mills, G.; Vaughan, J.K.; Draxler, R.R.; Rolph, G.; Ruminski, M.; Ferguson, S.A. Regional Real-Time Smoke Prediction Systems. In *Wildland Fires and Air Pollution. Development in Environmental Science*; Bytnerowicz, A., Arbaugh, M., Andersen, C., Riebau, A., Eds.; Elsevier: Amsterdam, The Netherlands, 2009; Volume 8, pp. 499–534.
4. Hodzic, A.; Madronich, S.; Bohn, B.; Massie, S.; Menut, L.; Wiedinmyer, C. Wildfire particulate matter in Europe during summer 2003: Meso-scale modeling of smoke emissions, transport and radiative effects. *Atmos. Chem. Phys.* **2007**, *7*, 4743–4764.
5. Wiedinmyer, C.; Quayle, B.; Geron, C.; Belote, A.; McKenzie, D.; Zhang, X.; O'Neill, S.M.; Wynne, K. Estimating emissions from fires in North America. *Atmos. Environ.* **2006**, *40*, 3419–3432.
6. Reid, J.S.; Hyer, E.J.; Prins, E.M.; Westphal, D.L.; Zhang, J.; Wang, J.; Christopher, S.A.; Curtis, C.A.; Schmidt, C.C.; Eleuterio, D.P.; *et al*. Global monitoring and forecasting of biomass-burning smoke: description of and lessons from the Fire Locating and Modeling of Burning Emissions (FLAMBE) program. *IEEE J. Sel. Top. Appl. Earth Obs. Remote Sens.* **2009**, *2*, 144–162.
7. Damoah, R.; Spichtinger, N.; Forster, C.; James, P.; Mattis, I.; Wandinger, U.; Beirle, S.; Wagner, T.; Stohl, A. Around the world in 17 days-hemispheric-scale transport of forest fire smoke from Russia in May 2003. *Atmos. Chem. Phys.* **2004**, *4*, 1311–1321.
8. Duck, T.J.; Firanski, B.J.; Millet, D.B.; Goldstein, A.H.; Allan, J.; Holzinger, R.; Worsnop, D.R.; White, A.B.; Stohl, A.; Dickinson, C.S. Transport of forest fire emissions from Alaska and the Yukon Territory to Nova Scotia during summer 2004. *J. Geophys. Res.* **2007**, *112*, D10S44:1–D10S44:13.
9. Trentmann, J.; Andreae, M.O.; Graf, H.-F.; Hobbs, P.V.; Ottmar, R.D.; Trautmann, T. Simulation of a biomass-burning plume: Comparison of model results with observations. *J. Geophys. Res.* **2002**, *107*, 4013:1–4013:15.
10. Freitas, S.R.; Longo, K.M.; Chatfield, R.; Latham, D.; Dias, M.A.F.S.; Andreae, M.O.; Prins, E.; Santos, J.C.; Gielow, R.; Carvalho, J.A., Jr. Including the sub-grid scale plume rise of vegetation fires in low resolution atmospheric transport models. *Atmos. Chem. Phys.* **2007**, *7*, 3385–3398.
11. Wooster, M.J.; Roberts, G.; Perry, G.L.W.; Kaufman, Y.J. Retrieval of biomass combustion rates and totals from fire radiative power observations: FRP derivation and calibration relationships between biomass consumption and fire radiative energy release. *J. Geophys. Res.* **2005**, *110*, D24311:1–D24311:24.
12. French, N.H.F.; Goovaerts, P.; Kasischke, E.S. Uncertainty in estimating carbon emissions from boreal forest fires. *J. Geophys. Res.* **2004**, *109*, D14S08:1–D14S08:12.

13. Breyfogle, S.; Ferguson, S.A. *User Assessment of Smoke-Dispersion Models for Wildland Biomass Burning*; U.S. Department of Agriculture, Forest Service, Pacific Northwest Research Station: Portland, OR, USA, 1996.
14. Turquety, S.; Logan, J.A.; Jacob, D.J.; Hudman, R.C.; Leung, F.Y.; Heald, C.L.; Yantosca, R.M.; Wu, S.; Emmons, L.K.; Edwards, D.P.; *et al*. Inventory of boreal fire emissions for North America in 2004: Importance of peat burning and pyroconvective injection. *J. Geophys. Res.* **2007**, *112*, D12S03:1–D12S03:13.
15. Duncan, B.N.; Strahan, S.E.; Yoshida, Y.B.; Steenrod, S.D.; Livesey, N. Model study of the cross-tropopause transport of biomass burning pollution. *Atmos. Chem. Phys.* **2007**, *7*, 3713–3736.
16. Guan, H.; Chatfield, R.B.; Freitas, S.R.; Bergstrom, R.W.; Longo, K.M. Modeling the effect of plume-rise on the transport of carbon monoxide over Africa with NCAR CAM. *Atmos. Chem. Phys.* **2008**, *8*, 6801–6812.
17. Hyer, E.J.; Chew, B.N. Aerosol transport model evaluation of an extreme smoke episode in Southeast Asia. *Atmos. Environ.* **2010**, *44*, 1422–1427.
18. Kahn, R.A.; Li, W.-H.; Moroney, C.; Diner, D.J.; Martonchik, J.V.; Fishbein, E. Aerosol source plume physical characteristics from space-based multiangle imaging. *J. Geophys. Res.* **2007**, *112*, D11205:1–D11205:20.
19. Labonne, M.; Bréon, F.M.; Chevallier, F. Injection height of biomass burning aerosols as seen from a spaceborne lidar. *Geophys. Res. Lett.* **2007**, *34*, L11806:1–L11806:5.
20. val Martin, M.; Logan, J.A.; Kahn, R.A.; Leung, F.Y.; Nelson, D.L.; Diner, D.J. Smoke injection heights from fires in North America: Analysis of 5 years of satellite observations. *Atmos. Chem. Phys.* **2010**, *10*, 1491–1510.
21. Guan, H.; Esswein, R.; Lopez, J.; Bergstrom, R.; Warnock, A.; Follette-Cook, M.; Fromm, M.; Iraci, L.T. A multi-decadal history of biomass burning plume heights identified using aerosol index measurements. *Atmos. Chem. Phys.* **2010**, *10*, 6461–6469.
22. Sessions, W.R.; Fuelberg, H.E.; Kahn, R.A.; Winker, D.M. An investigation of methods for injecting emissions from boreal wildfires using WRF-Chem during ARCTAS. *Atmos. Chem. Phys.* **2011**, *11*, 5719–5744.
23. Kahn, R.A.; Chen, Y.; Nelson, D.L.; Leung, F.-Y.; Li, Q.; Diner, D.J.; Logan, J.A. Wildfire smoke injection heights: Two perspectives from space. *Geophys. Res. Lett.* **2008**, *35*, L04809:1–L04809:4.
24. Winker, D.M.; Hunt, W.H.; McGill, M.J. Initial performance assessment of CALIOP. *Geophys. Res. Lett.* **2007**, *34*, L19803:1–L19803:5.
25. *Hazard Mapping System Fire and Smoke Product*; National Oceanic and Atmospheric Administration: Washington, DC, USA. Available online: http://www.osdpd.noaa.gov/ml/land/hms.html (accessed on 15 November 2011).
26. McNamara, D.P.; Stephens, G.; Ruminski, M.; Kasheta, T. The Hazard Mapping System (HMS)—NOAA's Multi-Sensor Fire and Smoke Detection Program Using Environmental Satellites. In *Proceedings of the 13th Conference on Satellite Meteorology and Oceanography*, Norfolk, VA, USA, 22 September 2004.

27. USDA Forest Service AirFire Team; Sonoma Technology Inc. BlueSky Gateway: SMARTFIRE. Available online: http://www.getbluesky.org/smartfire (accessed on 15 December 2011).
28. Raffuse, S.M.; Sullivan, D.C.; Chinkin, L.R.; Pryden, D.A.; Wheeler, N.J.M.; Larkin, N.K.; Solomon, R.; Soja, A. Integration and Reconciliation of Satellite-Detected and Incident Command-Reported Wildfire Information in the BlueSky Smoke Modeling Framework. In *Proceedings of the 6th Annual CMAS Conference*, Chapel Hill, NC, USA, 1-3 October 2007.
29. National Aeronautics and Space Administration; University of Alabama in Huntsville SMART and Sensor Webs. Available online: http://smartdev.itsc.uah.edu (accessed on 15 December 2011).
30. *CALIPSO Quality Statements*; National Oceanic and Atmospheric Administration: Washington, DC, USA. Available online: http://eosweb.larc.nasa.gov/PRODOCS/calipso/Quality_Summaries (accessed on 15 December 2011).
31. Winker, D.M.; Vaughan, M.A.; Omar, A.; Hu, Y.; Powell, K.A.; Liu, Z.; Hunt, W.H.; Young, S.A. Overview of the CALIPSO mission and CALIOP data processing algorithms. *J. Atmos. Ocean. Technol.* **2009**, *26*, 2310–2323.
32. *MISR Plume Height Project*; National Oceanic and Atmospheric Administration: Washington, D.C., USA. Available online: http://www.misr.jpl.nasa.gov/getData/accessData/MisrMinxPlumes/productDescription/ (accessed on 15 December 2011).
33. Nelson, D.L.; Chen, Y.; Kahn, R.A.; Diner, D.J.; Mazzoni, D. Example applications of the MISR INteractive eXplorer (MINX) software tool to wildfire smoke plume analyses. *Proc. SPIE* **2008**, *7089*, doi:10.1117/12.795087.
34. National Exposure Research Laboratory. *Science Algorithms of the EPA Models-3 Community Multiscale Air Quality (CMAQ) Modeling System*; U.S. Environmental Protection Agency: Research Triangle Park, NC, USA, 1999.
35. Hoelzemann, J.J.; Schultz, M.G.; Brasseur, G.P.; Granier, C.; Simon, M. Global Wildland Fire Emission Model (GWEM): Evaluating the use of global area burnt satellite data. *J. Geophys. Res.* **2004**, *109*, 4473–4475.
36. *BlueSky Framework,* version 3.0.0; U.S. Forest Service AirFire Team and Sonoma Technology, Inc.: Seattle, WA, USA, 2007.
37. Sullivan, D.C.; Raffuse, S.M.; Pryden, D.A.; Craig, K.J.; Reid, S.B.; Wheeler, N.J.M.; Chinkin, L.R.; Larkin, N.K.; Solomon, R.; Strand, T. *Development and Applications of Systems for Modeling Emissions and Smoke from Fires: The BlueSky Smoke Modeling Framework and SMARTFIRE*; Presented at the 17th International Emissions Inventory Conference: Portland, OR, USA, 5 June 2008.
38. *The Fuel Characteristic Classificaion System (FCCS)*, version 1; Fire and Environmental Research Applications Team: Seattle, WA, USA, 2007.
39. *Consume*, version 3.0; USDA Forest Service Fire and Environmental Research Applications Team: Seattle, WA, USA, 2005.
40. *Fire Emission Production Simulator (FEPS)*, version 1.1; Fire and Environmental Research Applications Team: Seattle, WA, USA, 2005.
41. *SMOKE*, version 2.3; Community Modeling and Analysis System at the University of North Carolina Chapel Hill: Chapel Hill, NC, USA, 2006.

42. *CMAQ*, version 4.5.1; Community Modeling and Analysis System at the University of North Carolina Chapel Hill: Chapel Hill, NC, USA, 2006.
43. Ottmar, R.D.; Sandberg, D.V.; Prichard, S.J.; Riccardi, C.L. *Fuel Characteristic Classification System*; Presented at the 2nd International Wildland Fire Ecology and Fire Management Congress: Orlando, FL, USA, 30 September 2004.
44. McKenzie, D.; Raymond, C.L.; Kellogg, L.K.B.; Norheim, R.A.; Andreu, A.G.; Bayard, A.C.; Kopper, K.E. Mapping fuels at multiple scales: Landscape application of the fuel characteristic classification system. *Can. J. Forest Res.* **2007**, *37*, 2421–2437.
45. Air Sciences, Inc. *Integrated Assessment Update and 2018 Emissions Inventory for Prescribed Fire, Wildfire, and Agricultural Burning*; Air Sciences, Inc.: Denver, CO, USA, 2005.
46. Briggs, G.A. Plume Rise Equations. In *Lectures on Air Pollution and Environmental Impact Analysis*; Haugen, D.A., Ed.; AMS: Boston, MA, USA, 1975; pp. 59–111.
47. Pasquill, F. The estimation of the dispersion of windborne material. *Meteorol. Mag.* **1961**, *90*, 33–49.
48. Coats, C.J. High Performance Algorithms in the Sparse Matrix Operator Kernel Emissions Modeling System. In *Proceedings of the 9th Joint Conference on Applications of Air Pollution Meteorology of the American Meteorological Society and the Air and Waste Management Association*, Atlanta, GA, USA, 28 January–3 February 1996.
49. Houyoux, M.R.; Adelman, Z. Quality Assurance Enhancements to the SMOKE Modeling System. In *Proceedings of the U.S. Environmental Protection Agency's International Emission Inventory Conference: One Atmosphere, One Inventory, Many Challenges*, Denver, CO, USA, 1–3 May 2001.
50. Houyoux, M.; Vukovich, J.; Brandmeyer, J. *Sparse Matrix Operator Kernel Emissions Modeling System (SMOKE) User Manual*; MCNC-North Carolina Supercomputing Center: Research Triangle Park, NC, USA, 2000.
51. Houyoux, M.R.; Vukovich, J.M. Updates to the Sparse Matrix Operator Kernel Emissions (SMOKE) Modeling System and Integration with Models-3. In *Proceedings of the Air & Waste Management Association's The Emission Inventory: Regional Strategies for the Future*, Raleigh, NC, USA, 26–28 October 1999.
52. Sessions, W.R.; Fuelberg, H.E.; Kahn, R.A.; Winker, D.M. An investigation of methods for injecting emissions from boreal wildfires using WRF-Chem during ARCTAS. *Atmos. Chem. Phys.* **2011**, *11*, 5719–5744.
53. Stephens, S.L. The application of service oriented software architectures in the fuels treatment community. *Int. J. Wildland Fire* **2005**, *14*, 213–222.
54. Liu, Y.; Achtemeier, G.L.; Goodrick, S.L.; Jackson, W.A. Important parameters for smoke plume rise simulation with Daysmoke. *Atmos. Pollut. Res.* **2010**, *1*, 250–259.
55. Freitas, S.R.; Longo, K.M.; Dias, S.; Chatfield, R.; Artaxo, P.; Andreae, M.O.; Grell, G.; Rodrigues, L.F.; Fazenda, A.; Panetta, J. The coupled aerosol and tracer transport model to the Brazilian developments on the regional atmospheric modeling system (CATT-BRAMS) Part 1: Model description and evaluation. *Atmos. Chem. Phys.* **2007**, *7*, 8525–8569.

56. Mazzoni, D.; Logan, J.A.; Diner, D.; Kahn, R.; Tong, L.; Li, Q. A data-mining approach to associating MISR smoke plume heights with MODIS fire measurements. *Remote Sens. Environ.* **2007**, *107*, 138–148.